Novel pyrimidine-benzimidazole hybrids with antibacterial and antifungal properties and potential inhibition of SARS-CoV-2 main protease and spike glycoprotein

Sharuk Khan[a*], Mayura Kale[b], Falak Siddiqui[a], Nitin Nema[c]

a. Department of Pharmaceutical Chemistry, MUP's College of Pharmacy (B Pharm), Washim, Maharashtra 444504, India
b. Department of Pharmaceutical Chemistry, Government College of Pharmacy, Aurangabad, Maharashtra 431003, India
c. Department of Pharmacology, Shri Vile Parle Kelavani Mandal's (SVKM's) Institute of Pharmacy, Dhule, Maharashtra 424001, India

A R T I C L E   I N F O

∗Corresponding author: Sharuk Khan, Assistant Protessor. Research direction: molecule designing and molecular docking studies followed by target selection.
E-mail: sharique.4u4@gmail.com.
Peer review under the responsibility of Hunan University of Chinese Medicine.

A B S T R A C T

Objective The study aimed to synthesize and characterize pyrimidine-linked benzimidazole hybrids, define their antimicrobial and antifungal activities *in vitro*, and determine their ability to inhibit the main protease and spike glycoprotein of SARS-CoV-2.

Methods The ability of the synthesized compounds to inhibit the main protease and spike glycoprotein inhibitory of SARS-CoV-2 was investigated by assessing their mode of binding to the allosteric site of the enzyme using molecular docking. The structures of pyrimidine-linked benzimidazole derivatives synthesized with microwave assistance were confirmed by spectral analysis. Antibacterial and antifungal activities were determined by broth dilution.

Results Gram-negative bateria (*Escherichia coli* and *Pseudomonas aeruginosa*) were more sensitive than gram-positive bateria (*Staphylococcus aureus* and *Streptococcus pyogenes*) to the derivatives. *Candida albicans* was sensitive to the derivatives at a minimal inhibitory concentration (MIC) of 250 μg/mL. The novel derivatives had better binding affinity (kcal/mol) than nelfinavir, lopinavir, ivermectin, remdesivir, and favipiravir, which are under investigation as treatment for SARS-CoV-2 infection. Compounds 2c, 2e, and 2g formed four hydrogen bonds with the active cavity of the main protease. Many derivatives had good binding affinity for the RBD of the of SARS-CoV-2 spike glycoprotein with the formation of up to four hydrogen bonds.

Conclusion We synthesized novel pyrimidine-linked benzi-midazole derivatives that were potent antimicrobial agents with ability to inhibit the SARS-CoV-2 spike glycoprotein. Understanding the pharmacophore features of the main protease

and spike glycoprotein offers much scope for the development of more potent agents. We plan to optimize the properties of the derivatives using models *in vivo* and *in vitro* so that they will serve as more effective therapeutic options against bacterial and SARS-CoV-2 infections.

1 Introduction

Coronavirus disease 2019 (COVID-19) [1] induced by the novel severe acute respiratory syndrome-related coronavirus (SARS-CoV-2) has been declared by the World Health Organization (WHO) as a pandemic [2]. Coronaviruses have triggered two other epidemics in addition to COVID-19, namely Middle East respiratory syndrome (MERS; 2012), and severe acute respiratory syndrome (SARS; 2002) [3]. The National Health Commission of China declared in January 20th, 2020 that SARS-CoV-2 infection is transmitted by person-to-person contact [4]. SARS-CoV-2 belongs to the same family *Betacoronaviruses*, as those that caused SARS and MERS [5, 6]. The novel coronavirus is a single-stranded positive-sense RNA with a diameter of 80 – 120 nm and 42 large viral RNA genomes [7]. Coronaviruses are categorized as alpha- (α-COV), beta- (β-COV), gamma- (γ-COV), and delta- (δ-COV) types [8]. Six of them have infected humans, and SARS-CoV-2 is the seventh after SARS-CoV and MERS-CoV [9]. Symptoms of SARS-CoV-2 infection include fever, cough, dyspnea, myalgia, fatigue, decreased leukocyte counts, and pneumonia. Although numerous clinical trials have evaluated possible therapies for SARS-CoV-2 infection [10, 11], treatment is not yet available for COVID-19 [12].

SARS-CoV-2 invades after binding to host cellular receptors [13, 14]. Host cell receptors and the receptor-binding domain (RBD) of SARS-CoV-2 might be viable targets of interest in treating SARS-CoV-2 infection [15]. Nucleocapsid (N), envelope (E), membrane (M), and spike (S) proteins comprise the structural proteins of SARS-CoV-2 [16, 17]. The spike protein consists of an RBD that specifically binds to human angiotensin-converting enzyme-2 (hACE-2), which leads to host cell invasion [14, 17]. Much investigative focus is presently directed towards developing specific novel inhibitors of the RBD or hACE-2.

Remdesivir is an approved treatment for COVID-19 [18]. Lopinavir and nelfinavir might inhibit SARS-CoV-2 viral protease, and a clinical trial of favipiravir is underway for treating pneumonia induced by SARS-CoV-2 [17]. Favipiravir is a purine nucleoside that disrupts viral RNA synthesis [1], and ivermectin inhibits the replication of SARS-CoV-2 *in vitro* [19]. Therefore, we used remdesivir, nelfinavir, lopinavir, favipiravir, and ivermectin along with the native ligand in the crystal structure of SARS-CoV-2 main protease, that is, N3 as reference moieties for molecular docking studies [20].

Heterocyclic compounds provide scaffolds upon which pharmacophores can assemble to yield potent and selective drugs [21]. Among these, benzimidazole heterocyclics have attracted attention because they are easy to synthesize and have a wide range of biological activities. The benzimidazole ring is an essential component of vitamin-B12 in the form of 5, 6-dimethyl-l-(alpha-D-ribofuranosyl) benzimidazole [22]. Various benzimidazole derivatives with human and veterinary anthelmintic [23], anti-ulcer [24], cardiotonic [25], antihypertensive [26], analgesic [27], anticonvulsant [28], anticancer [29] properties have been developed [30, 31]. Pyrimidines and their derivatives also have anticancer [32], anxiolytic [33], antioxidant [34], antiviral [35], antifungal [36], anticonvulsant [36], antidepressant, and antibacterial properties [37]. The United States Food and Drug Administration (USFDA) has approved many purine and pyrimidine derivatives for the management of cancer and viral diseases [38]. Pyrimidine-fused bicyclic heterocyclic agents have anticancer, antiviral, and many other biological activities.

To date, 147 pyrimidine-fused bicyclic heterocyclic drugs have been approved for clinical application or are currently being clinically administered. The USFDA has authorized 57 of them to treat various diseases, among which, 22 are currently being applied to treat various types of cancer [39]. The pyrimidine ring system is abundant in nature as substituted and ring-fused compounds and equivalents, such as cytosine, thymine, uracil, thiamine (vitamin B1) and alloxan. It is also found in various synthetic compounds, including barbiturates and the HIV

medication, zidovudine. Bacimethrin, a naturally occurring thiamine antimetabolite obtained in 1961 from *Bacillus megatherium*, is the most basic pyrimidine antibiotic, and it acts against many bacterial infections [40]. Pyrimidine-fused bicyclic heterocyclic compounds can serve as scaffolds to find new and effective medicines for specific biological targets.

The present study aimed to synthesize and characterize pyrimidine-linked benzimidazole hybrids with antimicrobial and antifungal activity as well as inhibitory activity against SARS-CoV-2 main protease and spike glycoprotein. We screened their antiviral inhibitory action by molecular docking *in silico* as we were unable to screen them for SARS-CoV-2 activity *in vivo* due to safety issues. We therefore investigated their antimicrobial and antifungal activities *in vitro* as preliminary evidence of their biological potential. Molecular docking *in silico* validates the binding affinity of compounds for target molecules as a docking scores (kcal/mol). This allows the prediction of structural activity relationships between compounds and targets.

2 Materials and methods

2.1 Molecular docking

Compounds were screened by molecular docking using the PyRx-Virtual Screening Tool [41] on a Lenovo ThinkPad with a 64-bit operating system, an Intel(R) Core™ i5-4300M processor with a base frequency of 2.60 GHz and 4GB RAM.

The structures of approved drugs remdesivir, lopinavir, nelfinavir, invermectin, favipiravir, and native ligand (Spatial Data File [SDF]) were downloaded from the U.S. National Library of Medicine, PubChem (https://pubchem.ncbi.nlm.nih.gov/), and the structures of 1,2,3,4-tetrahydropyrimidine-2-thiols and novel pyrimidine-linked benzimidazole derivatives were sketched in ChemDraw Ultra 8.0. Energy was minimized using a universal force field (UFF) [42]. We investigated the binding affinity of the derivatives for the SARS-CoV-2 main protease (PDB ID: 6LU7) and spike glycoprotein (6VSB). The crystal structures of 6LU7 (https://www.rcsb.org/structure/6LU7) and 6VSB (https://www.rcsb.org/structure/6VSB) were downloaded from the RCSB Protein Data Bank. The

native ligand in 6LU7 was N-[(5-methylisoxazol-3-yl) carbonyl] alanyl-L-valyl-N~1~-((1R, 2Z)-4-(benzyloxy)-4-oxo-1-{[(3R)-2-oxopyrrolidin-3-yl] methyl} but-2-enyl)-L-leucinamide [20]. The crystal structure of 6VSB did not indicate a native ligand. Molecular docking proceeded as described [43–45]. The interacting amino acid residues in the protein were identified using BIOVIA Discovery Studio Visualizer version 19.1.0.18287 (Dassault Systemes, Paris, France) [46].

2.2 Design of novel pyrimidine-linked benzimidazole hybrids

We designed derivatives by merging the 2-(chloromethyl)-1H-benzimidazole moiety with 1,2,3,4-tetrahydropyrimidine-2-thiol pyrimidine derivatives synthesized via the modified Biginelli reaction. Figure 1 shows the approach used to construct the derivatives. We then compared binding affinities of 1,2,3,4-tetrahydropyrimidine-2-thiols and novel pyrimidine-linked benzimidazole derivatives to determine the significance of merging the two moieties.

Table 1 shows structures of the pyrimidine derivatives and final novel derivatives obtained by merging benzimidazole with pyrimidine.

2.3 Laboratory procedures

2.3.1 Synthesis of 2-(chloromethyl)-1H-benzimidazole This procedure is described in the Supplementary material. The yield was 85%. A yellowish-brown product recrystallized from dioxane; m.p., 152 – 154 °C [compared with the literature: 147.8 – 148.2 °C] [47]. Care was taken while handling 2-(chloromethyl)-1H-benzimidazole because it is a powerful skin and mucous membrane irritant [48]. Figure 2 shows the reaction scheme for the synthesis of this compound.

2.3.2 Synthesis of pyrimidine derivatives The modified Biginelli reaction proceeded as described and detailed in the Supplementary material [49] and generated 1,2,3,4-tetrahydropyrimidine-2-thiol from ethyl acetoacetate, aldehyde, and thiourea [37, 50] at 75% – 95% yield (Figure 3).
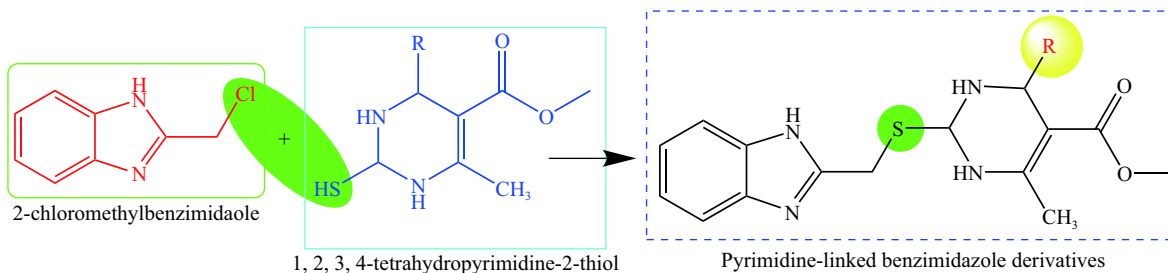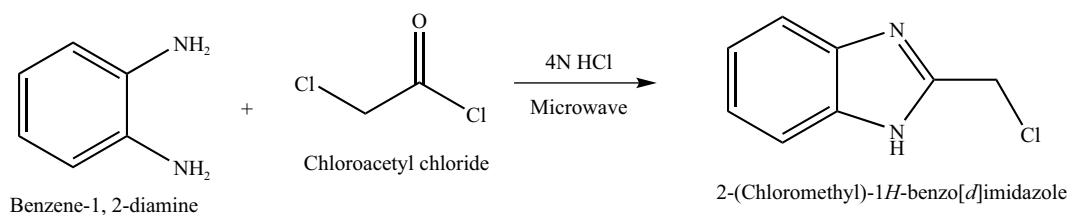

Figure 1 Synthesis of pyrimidine-linked benzimidazole scaffold

Table 1 Structures of 1,2,3,4-tetrahydropyrimidine-2-thiols and novel pyrimidine-linked benzimidazole derivatives

Code	Structure of 1,2,3,4-tetrahydropyrimidine-2-thiols	Code	Structure of pyrimidine-linked benzimidazole hybrids
1a		2a	
1b		2b	
1c		2c	
1d		2d	
1e		2e	
1f		2f	
1g		2g	
1h		2h	

Figure 2 Synthesis of 2-(chloromethyl)-1H-benzimidazole

2.3.3 Merging 2-(chloromethyl)-1H-benzimidazole and 1,2,3,4-tetrahydropyrimidine-2-thiols to synthesize pyrimidine-linked benzimidazole derivatives We condensed 2-(chloromethyl)-1H-benzimidazole (1.66 g, 0.01 mol and 1,2,3,4-tetrahydropyrimidine-2-thiol (0.01 mol) by heating with potassium hydroxide (KOH) and H_2O : acetone (2 : 1) at 50 – 60 °C for 45 min.

The reaction mixture was chilled to room temperature, decanted into ice-cold water, filtered, and recrystallized from ethanol (Figure 4). The yield was 90% – 95%.

2.4 Calculation of Lipinski rule of five

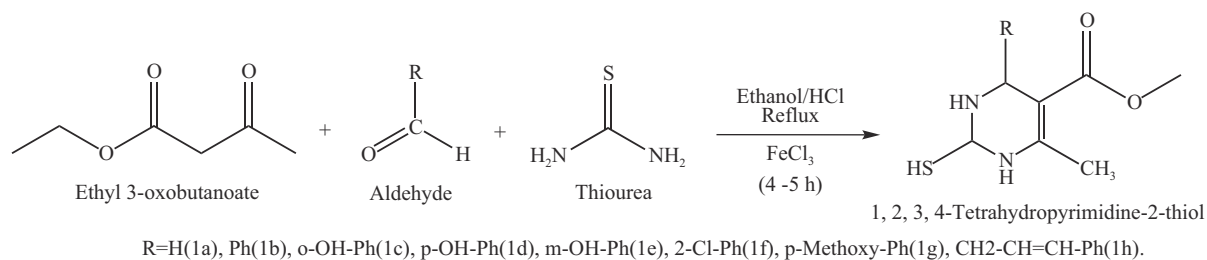We applied the Lipinski rule of five that defines the

R=H(1a), Ph(1b), o-OH-Ph(1c), p-OH-Ph(1d), m-OH-Ph(1e), 2-Cl-Ph(1f), p-Methoxy-Ph(1g), CH2-CH=CH-Ph(1h).

Figure 3 Synthesis of 1,2,3,4-tetrahydropyrimidine-2-thiols via modified Biginelli reaction

R=H (2a), Ph (2b), o-OH-Ph (2c), p-OH-Ph (2d), m-OH-Ph (2e), 2-Cl-Ph (2f), p-Methoxy-Ph (2g), CH2-CH=CH-Ph (2h)
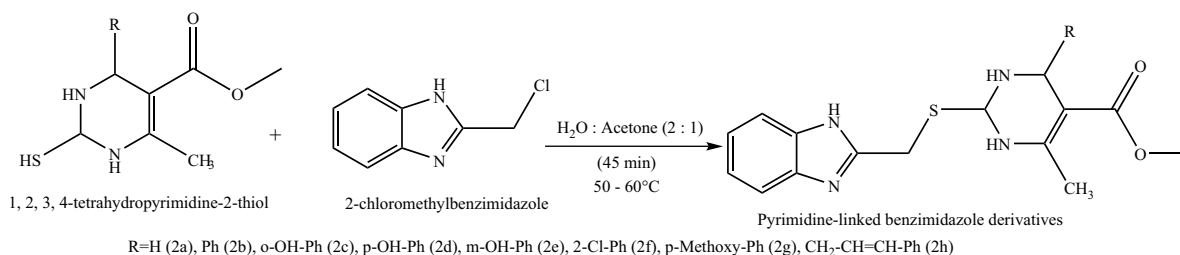
Figure 4 Synthesis of novel pyrimidine-linked benzimidazole derivatives

ability of new molecular entities to be useful drugs. In terms of drug development, the rule states that weak absorption or permeation is more likely when the criteria of > 5 H-bond donors, 10 H-bond acceptors, molecular weight > 500, and a measured $\text{Log} P (\text{MLog} P) > 5$ are met [51-54]. The properties of all derivatives were calculated using the SwissADME online tool (http://www.swissadme.ch/index.php).

2.5 Biological activity

Various concentrations of derivatives were prepared in DMSO to assess their antibacterial and antifungal activities against standard strains (Table 2) using broth dilution. Bacteria were maintained, and drugs were diluted in nutrient Mueller Hinton broth. The broth was inoculated with 10^8 colony-forming units (CFU) per milliliter of test strains (Institute of Microbial

Table 2 Bacterial and fungal strains for activity assay

Organism	International code
Escherichia coli (Gram-negative)	MTCC-443
Pseudomonas aeruginosa (Gram-negative)	MTCC-1688
Staphylococcus aureus (Gram-positive)	MTCC-96
Streptococcus pyogenes (Gram-positive)	MTCC-442
Candida albicans	MTCC-227
Aspergillus niger	MTCC-282
Aspergillus clavatus	MTCC-1323

Technology, Chandigarh, India) determined by turbidity. Stock solutions of synthesized derivates (2 mg/mL) were serially diluted for primary and secondary screening. The primary screen included 1 000, 500, and 250 μg/mL of synthesized derivatives, then those with activity were further screened at 200, 100, 50, 25, 12.5, and 6.250 μg/mL. A control without antibiotic was subcultured (before inoculation) by spreading one loopful evenly over a quarter of a plate of medium suitable for growing test organisms and incubated at 37 °C overnight. The lowest concentrations of derivatives that inhibited bacterial or fungal growth were taken as minimal inhibitory concentrations (MICs). These were compared with the amount of control growth before incubation (original inoculum) to determine MIC accuracy [55-57]. The standards for antibacterial activity were gentamycin, ampicillin, chloramphenicol, ciprofloxacin, and norfloxacin served, and those for antifungal activity were nystatin and griseofulvin.

3 Results

3.1 Molecular docking

Table 3 shows details of the SARS-CoV-2 main protease and spike glycoprotein according to PDB X-ray structure validation reports.

Table 4 shows details of the derivatives, their binding affinity (kcal/mol), number of hydrogen bonds formed with targets and active amino acid residues involved in interactions. Data for compounds 1a – 1h (1,2,3,4-tetrahydropyrimidine-2-thiols), are provided in Supplementary material.

Table 5 shows the two- and three-dimensional (2D and 3D) binding positions of the derivatives.

Table 3　Crystal structures of SARS-CoV-2 main protease (Mpro) and spike glycoprotein used for molecular docking

Particular	PDB ID	
	6LU7	6VSB
Title	The crystal structure of COVID-19 main protease in complex with an inhibitor N3	Prefusion 2019-nCoV spike glycoprotein with one receptor-binding domain up
DOI	10.2210/pdb6LU7/pdb	10.2210/pdb6VSB/pdb
Authors	LIU X, ZHANG B, JIN Z, YANG H, RAO Z	WRAPP D, WANG N, CORBETT KS, GOLDSMITH JA, HSIEH C, ABIONA O, GRAHAM BS, MCLELLAN JS
Deposited on	2020-01-26	2020-02-10
Resolution	2.16 Å (reported)	3.46 Å (reported)
Classification	Viral Protein	Viral Protein
Organism(s)	Bat SARS-like coronavirus	Severe acute respiratory syndrome coronavirus 2
Expression System	Escherichia coli BL21(DE3)	Homo sapiens
Method	X-Ray Diffraction	Electron Microscopy

Table 4　Details of the synthesized derivatives

Drug name or derivative code	6LU7			6VSB		
	Binding affinity (kcal/mol)	Hydrogen bonds (n)	Active amino acid residues	Binding affinity (kcal/mol)	Hydrogen bonds (n)	Active amino acid residues
Native ligand	– 9	7	Leu141, Phe140, Glu166, Gln192, Pro168, Gln189, Met49, His41, Arg188, Met165, Asp187, His164, Leu27, Thr25, Thr26, Thr24	–	–	–
Approved drugs for the treatment of SARS-CoV-2 infection　Nelfinavir	– 8	3	Leu27, Cys145, Asn142, Glu166, His164, His41, Tyr54, Asp187, Met165, Gln189, His163, His172, Phe140, Leu141, Ser144, Gly143, Thr26, Thr25	– 8.7	1	Gly-A:232, Arg-C:355, Phe-C:464
Lopinavir	– 7.3	2	Pro168, Glu166, Asn142, Ser46, Thr25, Thr26, Leu27, Cys145, Met49, His164, Asp187, His41, Arg188, Tyr54, Met165, Gln189	– 8.5	0	Arg-B:995, Asp-C:994, Thr-B:998, Arg-A:995, Thr-A:998, Tyr-B:756, Thr-C:998
Ivermectin	– 7.3	3	Asn85, Val186, Arg40, Asn53, Met82	– 9.1	4	Cys-C:379, Glu-A:988, Val-C:382, Pro-A:987, Val-A:991, Val-B:991, Lys-C:378

Table 4 Continued

Drug name or derivative code		6LU7			6VSB		
		Binding affinity (kcal/mol)	Hydrogen bonds (n)	Active amino acid residues	Binding affinity (kcal/mol)	Hydrogen bonds (n)	Active amino acid residues
Approved drugs for the treatment of SARS-CoV-2 infection	Remdesivir	− 7	8	Pro168, Leu167, Thr190, His172, Met165,Phe140, His163, Leu141, Ser144, His164, Cys145, Gly143, Met49, Asn142, Glu166, Gln189, Ala191	− 6.3	5	Asn-B:542, Thr-B:547, Asp-C:745, Leu-C:981, Thr-B:549, Lys-B:386, Leu-C:981
	Favipiravir	− 5.7	4	Gln127, Asp295, Phe08, Asn151, Phe112, Phe294, Thr292, Thr111, Gln110, Ile106	− 5.2	4	Asp-A:994, Phe-C:970, Arg-C:995, Thr-C:998, Gly-C:999
Novel pyrimidine-linked benzimidazole hybrids	2a	− 6.6	1	Thr190, Met165, His41, Glu166, His164, Met49, Cys145, Thr26, Gly143, Leu27, Thr25, Ser144, Leu141, Gln189	− 7.2	3	Thr-B:998, Thr-A:998, Asp-B:994, Tyr-B:756
	2b	− 7.1	2	Pro168, Asn142, His41, Met49, Asp187, Arg188, Tyr54, Met165, Gln189, Cys145, Leu167	− 7.9	2	Asp-B:994, Thr-B:998
	2c	− 7.8	4	His163, Asn142, His164, His41, Met165, Asp187, Arg188, Val186, Gln192, Thr190, Pro168, Gln189, Cys145, Met49, Thr25, Thr26, Leu27, Gly143, Leu141, Ser144	− 8.5	3	Asn-B:978, Leu-B:977, Thr-A:547, Val-B:976, Leu-A:546
	2d	− 7.6	3	Thr25, Leu27, Thr26, Gly143, Leu141, Gln189, Thr190, Met165, Glu166, His164, Arg188, Asp187, Met49	− 8.4	3	Thr-C:998, Asp-B:994, Arg-A:995, Thr-B:998, Tyr-C:756
	2e	− 7.4	4	Tyr54, Asp187, Met49, His164, Asn142, Leu167, Pro168, Thr190, Gln192, Glu166, Gln189, Met165, Arg188, His41	− 8.8	1	Thr-C:998, Tyr-C:756, Thr-B:998, Arg-A:995, Asp-B:994, Arg-C:995, Arg-B:995

Table 4 Continued

Drug name or derivative code	6LU7			6VSB		
	Binding affinity (kcal/mol)	Hydrogen bonds (*n*)	Active amino acid residues	Binding affinity (kcal/mol)	Hydrogen bonds (*n*)	Active amino acid residues
2f	− 8.1	1	His41, His164, Met165, Met49, Tyr54, Asp187, Arg188, Gln189, Thr190, Gln192, Leu167, Pro168, Leu141, Asn142, Cys145, Ser144, Gly143, Leu27	− 8.2	3	Thr-B:415, Gly-B:416, Gln-B:414, Pro-C:384, Glu-A:988, Asp-A:985, Thr-C:385
Novel pyrimidine-linked benzimidazole hybrids 2g	− 7.2	4	Cys145, His41, Met165, His164, Met49, Gln189, Glu166, Leu167, Pro168, Asn142, Leu141, Phe140, Arg188, Tyr54, His163, Asp187	− 8.3	4	Thr-A:998, Arg-A:995, Thr-C:998, Tyr-C:756, Thr-B:998, Thr-C:998
2h	− 8.0	2	Met165, Cys145, Ser144, Met49	− 8.3	1	Tyr-B:756, Thr-C:998, Thr-B:998. Tyr-C:756

These enabled us to predict which atoms and/or groups in a ligand are involved in interactions with amino acid residues in target derivatives. Details of 2D and 3D-docking of compounds 1a – 1h are provided in the Supplementary material.

Table 6 shows changes in the number of hydrogen bonds formed and binding affinity before and after merging with benzimidazole.

3.2 Chemistry

Spectral characterization revealed the formation of pyrimidine-linked benzimidazole derivatives. The chemistry, melting points, physical properties, and IR spectra are provided in the Supplementary material.

3.2.1 2-(chloromethyl)-1H-benzimidazole Molecular formula, $C_8H_7ClN_2$; molecular weight, 166.61; appearance, yellowish brown; soluble in ethanol, acetone, benzene; elemental analysis, C, 57.67; H, 4.23; Cl, 21.28; N, 16.81; Log *P*, 2.11; yield, 90%; m.p., 152 – 154 °C; IR: aromatic, 933 and 842 cm⁻¹; halogen, 642 cm⁻¹; NH bending, 1 600 cm⁻¹; NH stretching, 3 300 – 3 400 cm⁻¹; CH bending, 700 and 842 cm⁻¹; CH stretching, 3 084 cm⁻¹; C=C, 1 650 cm⁻¹.

3.2.2 Ethyl 1,2,3,4-tetrahydro-2-mercapto-6-methyl-pyrimidine-5-carboxylate (1a) Molecular formula, $C_8H_{14}N_2O_2S$; molecular weight, 198.24; appearance, light pink powder; soluble in ethanol, acetone, benzene; m/e ratio, 198.05 (100.0%), 199.05 (9.6%), 200.04 (4.5%); elemental analysis, C, 48.47; H, 5.08; N, 14.13; O, 16.14; S, 16.17; Log *P*, 1.66; yield, 80%; m.p., 213 – 215 °C; IR: NH bending, 1 600 cm⁻¹; NH stretching, 3 315 cm⁻¹; CH bending, 960 cm⁻¹; CH stretching, 3 030 cm⁻¹; ester group, 1 710 cm⁻¹; SH stretching, 2 524 cm⁻¹; C-S stretching, 680 cm⁻¹; aromatic, 690 cm⁻¹.

3.2.3 Ethyl-1,2,3,4-tetrahydro-2-mercapto-6-methyl-4-phenylpyrimidine-5-carboxylate (1b) Molecular formula, $C_{14}H_{18}N_2O_2S$; molecular weight, 274.34; appearance, milky white crystals; soluble in ethanol, acetone, benzene; m/e ratio, 274.08 (100.0%), 275.08 (16.2%), 276.07 (4.5%), 276.08 (1.7%); elemental analysis, C, 61.29; H, 5.14; N, 10.21; O, 11.66; S, 11.69; Log *P*, 3.76; yield 85%; m.p., 203 – 205 °C; IR: NH bending 1 654 cm⁻¹; NH stretching, 3 332 cm⁻¹; CH bending, 869 cm⁻¹; CH stretching, 3 180 cm⁻¹; ester group, 1 700 cm⁻¹; aromatic, 700 cm⁻¹; SH stretching, 2 582 cm⁻¹; C-S stretching 692 cm⁻¹.

3.2.4 Ethyl-1,2,3,4-tetrahydro-4-(2-hydroxyphenyl)-2-mercapto-6-methylpyrimidine-5-carboxylate (1c) Molecular formula, $C_{14}H_{18}N_2O_3S$; molecular weight, 290.34; appearance, prismatic white crystals; soluble in

Table 5 2D and 3D docking positions of drugs targeting SARS-CoV-2 main protease and RBD of spike glycoprotein
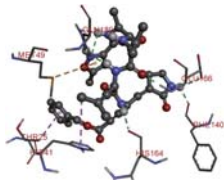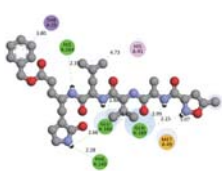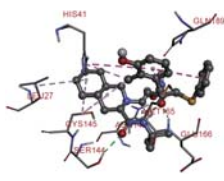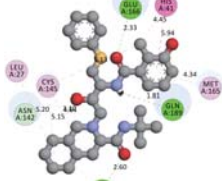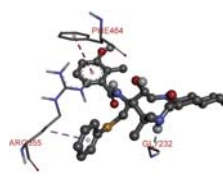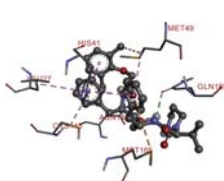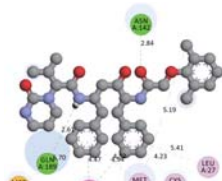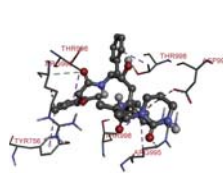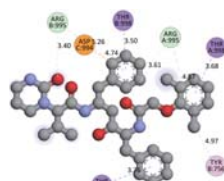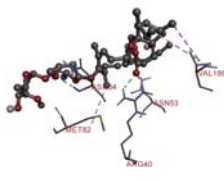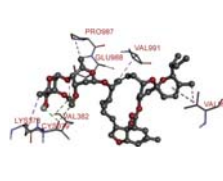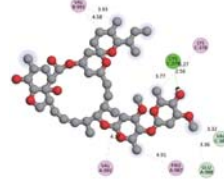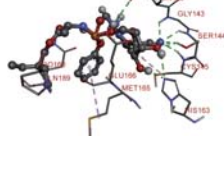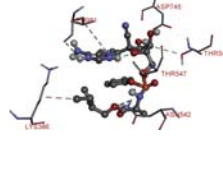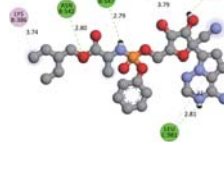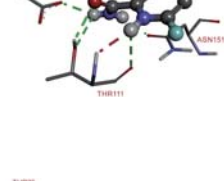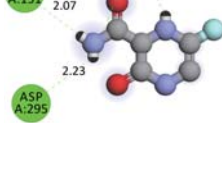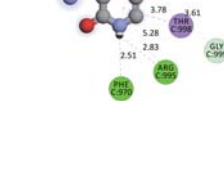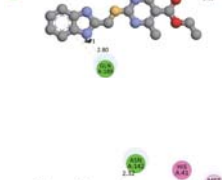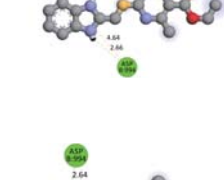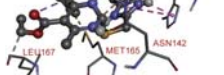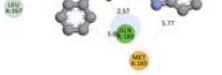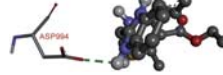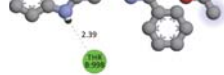
Compound derivative code	6LU7		6VSB	
	3D	2D	3D	2D
Native ligand			−	−
Nelfinavir				
Lopinavir				
Ivermectin				
Remdesivir				
Favipiravir				
2a				
2b				

Table 5 Continued

Compound derivative code	6LU7		6VSB	
	3D	2D	3D	2D
2c				
2d				
2e				
2f				
2g				
2h				

in ethanol, acetone, benzene; m/e ratio, 290.07 (100.0%), 291.08 (15.4%), 292.07 (4.6%), 292.08 (1.8%), 291.07 (1.5%; elemental analysis, C, 57.92; H, 4.86; N, 9.65; O, 16.53; S, 11.04; Log P, 3.37; yield, 77%; m.p., 201 – 203 °C; IR: NH bending, 1 581 cm^{-1}; NH stretching, 3 300 cm^{-1}; CH bending, 756 cm^{-1}; CH stretching, 3 003 cm^{-1}; ester group, 1 751 cm^{-1}; hydroxy group, 3 600 cm^{-1}; aromatic o-disubstituted, 730 cm^{-1}; SH stretching, 2 600 cm^{-1}; C-S stretching, 650 cm^{-1}.

3.2.5 Ethyl-1,2,3,4-tetrahydro-4-(3-hydroxyphenyl)-2-mercapto-6-methylpyrimidine-5-carboxylate (1d)

Molecular formula, $C_{14}H_{18}N_2O_3S$; molecular weight, 290.34; appearance, light brown powder; soluble in ethanol, acetone, benzene; m/e ratio, 290.07 (100.0%), 291.08 (15.4%), 292.07 (4.6%), 292.08 (1.8%), 291.07 (1.5%); elemental analysis, C, 57.92; H, 4.86; N, 9.65; O, 16.53; S, 11.04; Log P, 3.37; yield, 79%; m.p., 179 – 181 °C; IR: -NH bending, 1 610 cm^{-1}; NH stretching, 3 319 cm^{-1}; CH bending, 866 cm^{-1}; CH

Table 6 Affinity and hydrogen bonds formed after pyrimidine-linked benzimidazole hybrids bound to SARS-CoV-2 main protease

Code	1,2,3,4-tetrahydropyrimidine-2-thiols		Code	Pyrimidine-linked benzimidazole hybrids	
	Binding affinity (kcal/mol)	Hydrogen bonds (n)		Binding affinity (kcal/mol)	Hydrogen bonds (n)
1a	− 4.4	4	2a	− 6.6	1
1b	− 6.1	1	2b	− 7.1	2
1c	− 5.8	2	2c	− 7.8	4
1d	− 6.1	3	2d	− 7.6	3
1e	− 6.1	3	2e	− 7.4	4
1f	− 5.9	1	2f	− 8.1	1
1g	− 6.1	1	2g	− 7.2	4
1h	− 6.3	1	2h	− 8.0	2

stretching 3 150 cm^{-1}; ester group 1 700 cm^{-1}; hydroxy group, 3 600 cm^{-1} aromatic m-disubstituted, 680 and 788 cm^{-1}; SH stretching, 2 500 cm^{-1}; C-S stretching, 630 cm^{-1}.

3.2.6 Ethyl-1,2,3,4-tetrahydro-4-(4-hydroxyphenyl)-2-mercapto-6-methylpyrimidine-5-carboxylate (1e)

Molecular formula, $C_{14}H_{14}N_2O_3S$; molecular weight, 290.34; appearance, off-white powder; soluble in ethanol, acetone, benzene; m/e ratio, 290.07 (100.0%), 291.08 (15.4%), 292.07 (4.6%), 292.08 (1.8%), 291.07 (1.5%); elemental analysis, C, 57.92; H, 4.86; N, 9.65; O, 16.53; S, 11.04; Log P, 3.37; yield, 85%; m.p., 225 – 227 °C; IR: NH bending, 1 581 cm^{-1}; NH stretching 3 400 cm^{-1}; SH bending, 825 cm^{-1}; SH stretching 3 016 and 3 196 cm^{-1}; ester group 1 689 cm^{-1}; hydroxy group 3 502 cm^{-1} aromatic p-disubstituted, 825 cm^{-1}; SH stretching, 2 561 cm^{-1}; C-S stretching, 642 cm^{-1}.

3.2.7 Ethyl-4-(2-chlorophenyl)-1,2,3,4-tetrahydro-2-mercapto-6-methylpyrimidine-5-carboxylate (1f)

Molecular formula, $C_{14}H_{17}ClN_2O_2S$; molecular weight, 308.78; appearance, yellowish white sticky product; soluble in ethanol, acetone, benzene; m/e ratio, 308.04 (100.0%), 310.04 (32.6%), 309.04 (16.9%), 311.04 (5.9%), 310.03 (4.5%), 312.03 (1.5%), 310.05 (1.1%); elemental analysis, C, 54.46; H, 4.24; Cl, 11.48; N, 9.07; O, 10.36; S, 10.38; Log P, 4.31; yield, 87%; m.p. 192 – 194 °C; IR: NH bending, 1 580 cm^{-1}; NH stretching, 3 350 cm^{-1}; CH bending, 767 cm^{-1}; CH stretching, 3 100 cm^{-1}; ester group, 1 724 cm^{-1}; halogen group, 646 cm^{-1}; aromatic o-disubstituted, 767 cm^{-1}; SH stretching, 2 349 cm^{-1}; C-S stretching, 646 cm^{-1}.

3.2.8 Ethyl-1,2,3,4-tetrahydro-2-mercapto-4-(4-methoxyphenyl)-6-methylpyrimidine-5-carboxylate (1g)

Molecular formula, $C_{15}H_{20}N_2O_3S$; molecular weight, 304.36; appearance, white crystals; soluble in ethanol, acetone, benzene; m/e ratio, 304.09 (100.0%), 305.09 (18.1%), 306.08 (4.5%), 306.09 (2.1%); elemental analysis, C, 59.19; H, 5.30; N, 9.20; O, 15.77; S, 10.54; Log P, 3.63; yield, 92%; m.p., –199 – 201 °C; IR: NH bending, 1 581 cm^{-1}; NH stretching, 3 319 cm^{-1}; CH bending, 767 cm^{-1}; CH stretching, 3 150 cm^{-1}; ester group, 1 710 cm^{-1}; ether group, 1 186 cm^{-1}; aromatic p-disubstituted, 790 cm^{-1}; SH stretching, 2 500 cm^{-1}; C-S stretching, 653 cm^{-1}.

3.2.9 Ethyl-4-cinnamyl-1,2,3,4-tetrahydro-2-mercapto-6-methylpyrimidine-5-carboxylate (1h)

Molecular formula, $C_{17}H_{22}N_2O_2S$; molecular weight, 314.4; appearance, white crystals; soluble in ethanol, acetone, benzene; m/e ratio, 314.11 (100.0%), 315.11 (20.0%), 316.10 (4.5%), 316.12 (1.6%); Elemental Analysis, C, 64.94; H, 5.77; N, 8.91; O, 10.18; S, 10.20; Log P, 4.55; yield, 82%; m.p., 200 – 202 °C; IR, NH bending, 1 595 cm^{-1}; NH stretching, 3 400 cm^{-1}; CH bending, 852 cm^{-1}; CH stretching, 3 150 cm^{-1}; ester group, 1 703 cm^{-1}; C =C, 1 670 cm^{-1}; aromatic, monosubstituted, 700 and 770 cm^{-1}; SH stretching, 2 600 cm^{-1}; SH stretching, 661 cm^{-1}.

3.2.10 Ethyl-2-((1H-benzo[d]imidazol-2-yl)methylthio)-1,2,3,4-tetrahydro-6-methylpyrimidine-5-carboxylate (2a)

Molecular formula, $C_{16}H_{20}N_4O_2S$; molecular weight, 328.39; appearance, yellowish brown; soluble in ethanol, acetone, benzene; m/e ratio, 328.10 (100.0%), 329.10 (19.7%), 330.10 (5.3%), 330.11 (1.5%); elemental analysis, C, 58.52; H, 4.91; N, 17.06; O, 9.74; S, 9.76; Log P, 3.07; yield, 91%; m.p., 172 – 174 °C; IR: NH bending, 1 546 cm^{-1}; NH stretching, 3 313 cm^{-1}; CH bending, 750 cm^{-1}; CH stretching, 3 034 cm^{-1}; ester group, 1 700 cm^{-1}; C =C, 1 600 cm^{-1}; aromatic, 750 cm^{-1}; -C-S-C, 750 cm^{-1}; C-S stretching, 680 cm^{-1}.

3.2.11 Ethyl-2-((1H-benzo[d]imidazol-2-yl)methylthio)-1,2,3,4-tetrahydro-6-methyl-4-phenylpyrimidine-5-carboxylate (2b)

Molecular formula, $C_{22}H_{24}N_4O_2S$; molecular weight, 404.48; appearance, yellowish brown; soluble in ethanol, acetone, benzene; m/e ratio, 404.13 (100.0%), 405.13 (26.1%), 406.13 (5.5%), 406.14 (2.8%), 407.13 (1.1%); elemental analysis, C, 65.33; H, 4.98; N, 13.85; O, 7.91; S, 7.93; Log P, 5.17; yield, 93%; m.p., 142 – 144 °C; IR, NH bending, 1600 cm^{-1}; NH stretching, 3313 cm^{-1}; CH bending, 842 cm^{-1}; CH stretching, 3061 cm^{-1}; ester group, 1700 cm^{-1}; C=C, 1600 cm^{-1}; aromatic, 700 and 742 cm^{-1}; C = N group, 1644 cm^{-1}; -C-S-C, 742 cm^{-1}; C-S stretching, 700 cm^{-1}.

3.2.12 Ethyl-2-((1H-benzo[d]imidazol-2-yl)methylthio)-1,2,3,4-tetrahydro-4-(2-hydroxyphenyl)-6-methylpyrimidine-5-carboxylate (2c)

Molecular formula, $C_{22}H_{24}N_4O_3S$; molecular weight, 420.48; appearance, yellowish brown; soluble in ethanol, acetone, benzene; m/e ratio, 420.13 (100.0%), 421.13 (24.1%), 422.12 (4.5%), 422.13 (3.9%), 421.12 (2.3%), 423.12 (1.1%); elemental analysis, C, 62.84; H, 4.79; N, 13.32; O, 11.41; S, 7.63; Log P, 4.78; yield, 95%; m.p., 152 – 154 °C; IR: NH bending, 1593 cm^{-1}; NH stretching, 3313 cm^{-1}; CH bending, 700 cm^{-1}; CH stretching, 3055 cm^{-1}; ester group, 1764 cm^{-1}; C=C, 1600 cm^{-1}; aromatic o-disubstituted, 700 and 746 cm^{-1}; C = N group, 1670 cm^{-1}; C-S-C, 746 cm^{-1}; C-S stretching, 600 cm^{-1}.

3.2.13 Ethyl-2-((1H-benzo[d]imidazol-2-yl)methylthio)-1,2,3,4-tetrahydro-4-(3-hydroxyphenyl)-6-methylpyrimidine-5-carboxylate (2d)

Molecular formula, $C_{22}H_{24}N_4O_3S$; molecular weight, 420.48; appearance, yellowish brown; soluble in ethanol, acetone, benzene; m/e ratio, 420.13 (100.0%), 421.13 (24.1%), 422.12 (4.5%), 422.13 (3.9%), 421.12 (2.3%), 423.12 (1.1%); elemental analysis, C, 62.84; H, 4.79; N, 13.32; O, 11.41; S, 7.63; Log P, 4.78; yield, 95%; m.p., 223 – 225 °C; IR: NH bending, 1595 cm^{-1}; NH stretching, 3300 cm^{-1}; CH bending, 700 cm^{-1}; CH stretching, 3050 cm^{-1}; ester group, 1700 cm^{-1}; C=C, 1600 cm^{-1}; aromatic m-disubstituted, 700 and 742 cm^{-1}; C = N group, 1595 cm^{-1}; -C-S-C, 742 cm^{-1}; C-S stretching, 700 cm^{-1}.

3.2.14 Ethyl-2-((1H-benzo[d]imidazol-2-yl)methylthio)-1,2,3,4-tetrahydro-4-(4-hydroxyphenyl)-6-methylpyrimidine-5-carboxylate (2e)

Molecular formula, $C_{22}H_{24}N_4O_3S$; molecular weight, 420.48; appearance, yellowish brown; soluble in ethanol, acetone, benzene; m/e ratio, 420.13 (100.0%), 421.13 (24.1%), 422.12 (4.5%), 422.13 (3.9%), 421.12 (2.3%), 423.12 (1.1%); elemental analysis, C, 62.84; H, 4.79; N, 13.32; O, 11.41; S, 7.63; Log P, 4.78; yield, 96%; m.p., 138 – 140 °C; IR: NH bending, 1598 cm^{-1}; NH stretching, 3400 cm^{-1}; CH bending, 850 cm^{-1}; CH stretching, 3062 cm^{-1}; ester group, 1700 cm^{-1}; C=C, 1598 cm^{-1}; aromatic p-disubstituted, 742 cm^{-1}; C-S-C, 742 cm^{-1}; C-S stretching, 690 cm^{-1}.

3.2.15 Ethyl-2-((1H-benzo[d]imidazol-2-yl)methylthio)-4-(2-chlorophenyl)-1,2,3,4-tetrahydro-6-methylpyrimidine-5-carboxylate (2f)

Molecular formula, $C_{22}H_{23}ClN_4O_2S$; molecular weight, 438.93; appearance, yellowish brown; soluble in ethanol, acetone, benzene; m/e ratio, 438.09 (100.0%), 440.09 (37.0%), 439.10 (24.1%), 441.09 (9.5%), 440.10 (3.2%), 439.09 (2.3%), 442.08 (1.4%); elemental analysis, C, 60.20; H, 4.36; Cl, 8.08; N, 12.76; O, 7.29; S, 7.31; Log P, 5.73; yield, 90%; m.p., 106 – 108 °C; IR: NH bending, 1571 cm^{-1}; NH stretching, 3298 cm^{-1}; CH bending, 700 cm^{-1}; CH stretching, 2950 cm^{-1}; ester group, 1700 cm^{-1}; C=C, 1470 cm^{-1}; C=N group, 1691 cm^{-1}; halogen, 700 cm^{-1}; aromatic o-disubstituted, 752 cm^{-1}; -C-S-C, 752 cm^{-1}; C-S stretching, 650 cm^{-1}.

3.2.16 Ethyl-2-((1H-benzo[d]imidazol-2-yl)methylthio)-1,2,3,4-tetrahydro-4-(2-methoxyphenyl)-6-methylpyrimidine-5-carboxylate (2g)

Molecular formula, $C_{23}H_{26}N_4O_3S$; molecular weight, 434.51; appearance, yellowish brown; soluble in ethanol, acetone, benzene; m/e ratio, 434.14 (100.0%), 435.14 (27.2%), 436.14 (5.1%), 436.15 (3.7%), 437.14 (1.2%); elemental analysis, C, 63.58; H, 5.10; N, 12.89; O, 11.05; S, 7.38; Log P, 5.04; yield, 92%; m.p., 148 – 150 °C; IR: NH bending, 1590 cm^{-1}; NH stretching, 3300 cm^{-1}; CH bending, 833 cm^{-1}; CH stretching, 3150 cm^{-1}; ester group, 1699 cm^{-1}; ether, 1184 cm^{-1}; C=C, 1450 cm^{-1}; C = N group, 1680 cm^{-1}; aromatic p-disubstituted, 800 cm^{-1}; C-S-C, 744 cm^{-1}; C-S stretching, 650 cm^{-1}.

3.2.17 Ethyl-2-((1H-benzo[d]imidazol-2-yl)methylthio)-4-cinnamyl-1,2,3,4-tetrahydro-6-methylpyrimidine-5-carboxylate (2h)

Molecular formula, $C_{25}H_{28}N_4O_2S$; molecular weight, 444.55; appearance, yellowish brown; solubility, ethanol, acetone, benzene; m/e ratio, 444.16 (100.0%), 445.17 (27.4%), 446.16 (5.2%), 446.17 (4.0%), 445.16 (2.3%), 447.16 (1.2%); elemental analysis, C, 67.54; H, 5.44; N, 12.60; O, 7.20; S, 7.21; Log P, 5.04; yield, 90%; m.p., 180 – 182 °C; IR: NH bending, 1564 cm^{-1}; NH stretching, 3250 cm^{-1}; CH bending, 850 cm^{-1}; CH stretching, 3059 cm^{-1}; ester group, 1700 cm^{-1}; C = C, 1480 cm^{-1}; C = N group, 1680 cm^{-1}; aromatic mono-substituted, 694 cm^{-1}; -C-S-C, 746 cm^{-1}; C-S stretching, 694 cm^{-1}.

3.3 Antimicrobial and antifungal activity

The antimicrobial susceptibility of all synthesized

pyrimidine-linked benzimidazole derivatives was tested. Table 7 shows the MIC and minimum fungicidal concentrations (MFCs). The MIC of derivative 2a against *E. coli* was 62.5 μg/mL, which was much more potent than ampicillin, whereas derivatives 2c, 2e, and 2f were equipotent at a MIC of 100 μg/mL. *Pseudomonas aeruginosa* was sensitive to all synthesized derivatives at 62.5, 100, and 250 μg/mL, but not to ampicillin. *Staphylococcus aureus* was sensitive to derivatives 2a, 2b, 2d, 2e, and 2g at 200, 100, 100, 100, and 200 μg/mL, respectively, indicating that they were more potent than ampicillin, which was active at 250 μg/mL. The MICs of derivatives 2b

and 2f were both 100 μg/mL, and these compounds were equipotent against *S. pyogenes*. Derivatives 2b, 2c, 2d, 2e, and 2f exerted more effective fungicidal activity against *C. albicans* compared with griseofulvin with MICs of 250 and 500 μg/mL, respectively.

We used nystatin and griseofulvin as the standard antifungals against *A. niger*, *C. albicans*, and *A. clavatus*. Table 7 shows the MFCs. Derivatives 2b, 2c, 2d, 2e, and 2f exerted fungicidal activity against, *C. albicans* was sensitive at a MIC of 250 μg/mL compared with griseofulvin at 500 μg/mL.

Table 7 Minimum inhibitory and fungicidal concentrations of standard drugs and synthesized derivatives (μg/mL)

Drug name or code	E. coli	P. aeruginosa	S. aureus	S. pyogenes	C. albicans	A. niger	A. clavatus
2a	62.5	100	200	200	1 000	>1 000	>1 000
2b	125	62.5	100	100	250	500	500
2c	100	100	250	250	250	>1 000	>1 000
2d	250	100	100	250	250	>1 000	>1 000
2e	100	250	100	250	250	>1 000	>1 000
2f	100	62.5	250	200	250	500	500
2g	250	100	200	100	500	250	250
2h	250	250	250	500	500	250	250
Gentamycin	0.05	1	0.25	0.5	NA	NA	NA
Ampicillin	100	–	250	100	NA	NA	NA
Chloramphenicol	50	50	50	50	NA	NA	NA
Ciprofloxacin	25	25	50	50	NA	NA	NA
Norfloxacin	10	10	10	10	NA	NA	NA
Nystatin	NA	NA	NA	NA	100	100	100
Griseofulvin	NA	NA	NA	NA	500	100	100

NA represents not applicable.

3.4 Lipinski rule of five

None of the derivatives violated the rule of 5, indicating good absorption or permeation of the derivatives (Table 8).

4 Discussion

We applied molecular docking to compare the ability of pyrimidine-linked benzimidazole hybrids to inhibit SARS-CoV-2 main protease and the RBD of spike glycoprotein with approved drugs and native ligands. The binding affinity of several derivatives was similar to that of approved drugs. The formation

of a hydrogen bonds with target molecules results in inhibition, but binding affinity can be increased by van der Waals forces, Pi-Pi, and hydrophobic interactions. Thus, optimal inhibitors should comprise ligands that form hydrogen bonds with targets. For example, the binding affinity of remdesivir for the main protease is – 7 kcal/mol, which is much lower than that of approved drugs, but it forms about eight hydrogen bonds with target, which confers better inhibitory activity than these drugs. This could explain why it has been accepted for clinical trials for the management of COVID-19. Our novel derivatives also formed hydrogen bonds with their targets, indicating inhibitory potency

Table 8 Lipinski rule of five for all synthesized derivatives

Drug name or code	Molecular formula	Lipinski rule of five				Violation
		Molecular weight	HBA	HBD	Log P	
Native ligand (6LU7)	$C_{35}H_{48}N_6O_8$	680.7	9	5	0.38	1
Nelfinavir	$C_{32}H_{45}N_3O_4S$	567.8	5	4	3.20	1
Lopinavir	$C_{37}H_{48}N_4O_5$	628.8	5	4	2.93	1
Ivermectin	$C_{47}H_{72}O_{14}$	875.1	14	3	1.25	2
Remdesivir	$C_{27}H_{35}N_6O_8P$	602.6	12	4	0.18	2
Favipiravir	$C_5H_4FN_3O_2$	157.1	4	2	-1.30	0
2a	$C_{16}H_{20}N_4O_2S$	332.4	4	3	1.23	0
2b	$C_{22}H_{24}N_4O_2S$	408.5	4	3	2.39	0
2c	$C_{22}H_{24}N_4O_3S$	424.5	5	4	1.86	0
2d	$C_{22}H_{24}N_4O_3S$	424.5	5	4	1.86	0
2e	$C_{22}H_{24}N_4O_3S$	424.5	5	4	1.86	0
2f	$C_{22}H_{23}ClN_4O_2S$	442.9	4	3	2.87	0
2g	$C_{23}H_{26}N_4O_3S$	438.5	5	3	2.07	0
2h	$C_{25}H_{28}N_4O_2S$	448.5	4	3	2.95	0

towards the SARS-CoV-2 main protease.

The binding affinity of our novel derivatives for the RBD of the SARS-CoV-2 spike glycoprotein was as good that that of the approved drugs. The binding affinity of ivermectin for the RBD of SARS-CoV-2 spike glycoprotein is – 9.1 kcal/mol and it forms four hydrogen bonds. It interacts with Cys-C at 379, Glu-A at 988, Val-C at 382, Pro-A at 987, Val-A at 991, Val-B at 991, and Lys-C at 378. The binding affinity of remdesivir is – 6.3 kcal/mol and it forms five hydrogen bonds with the RBD. It interacts with Asn-B at 542, Thr-B at 547, Asp-C at 745, Leu-C at 981, Thr-B at 549, Lys-B at 386, and Leu-C at 981. Favipiravir forms four hydrogen bonds with the RBD and its binding affinity is – 5.2 kcal/mol. It interacts with Asp-A at 994, Phe-C at 970, Arg-C at 995, Thr-C at 998, and Gly-C at 999. Ivermectin, remdesivir, and favipiravir are currently applied to treat SARS-CoV-2 infection. Several of our derivatives have good binding affinity and formed up to four hydrogen bonds with the RBD of the SARS-CoV-2 spike glycoprotein.

Antimicrobial screening revealed that compounds with an aromatic ring at the R position were more potent than ampicillin, which is the standard antimicrobial against *P. aeruginosa*, *S. aureus*, and *S. pyogenes*. This might be attributed to the polar effect of the aromatic rings. Derivatives without substitution at the R position were more potent than ampicillin against *E. coli* and *S. aureus*, which might have been due to being smaller and having a low molecular weight. Compounds with phenyl, hydroxy phenyl, and chlorophenyl substitutions at the R position were more active than griseofulvin against *C. albicans*.

The drug-likeliness of ligands was assessed using Lipinski's rule of five in order to determine the pharmacokinetic characteristics of the synthesized ligands. All ligands were recognized as drug-like compounds and without any structural caution the physicochemical filter was passed through. The virtual screening method has the advantage of being able to produce ligands with high predicted binding affinities for completely new protein sequences. Here from the binding affinity, we can choose few potential ligands for the further optimization and development of novel anti-SARS-CoV-2 drugs. Compound 2c, 2d, 2e, 2f, 2g, and 2h exhibited good binding affinity with main protease and RBD of spike glycoprotein, also formed enough number of hydrogen bonds. We can choose these ligands for further optimization and validation, in order to search for more novel compounds for the treatment of COVID-19.

We determined changes in the binding affinity of pyrimidines after combining them with benzimidazole to predict the contributions of functional groups. The numbers of hydrogen bonds also changed, indicating the significance of merging benzimidazole with pyrimidine.

The docking scores of almost all derivatives indicated that binding affinity increased when merged with benzimidazole. Compound 1a formed four

hydrogen bonds and 2a formed only one with the SARS-CoV-2 main protease. Compounds 2c, 2d, 2e, 2f, and 2 g had better binding affinity and formed more hydrogen bonds than compound 2b, indicating that synthesized derivatives with different substituted benzaldehydes, preferably at the ortho and meta positions, would generate more potent derivatives. The binding affinity of compound 2h increased and it formed two hydrogen bonds, indicating that increasing the chain length of the R group increases
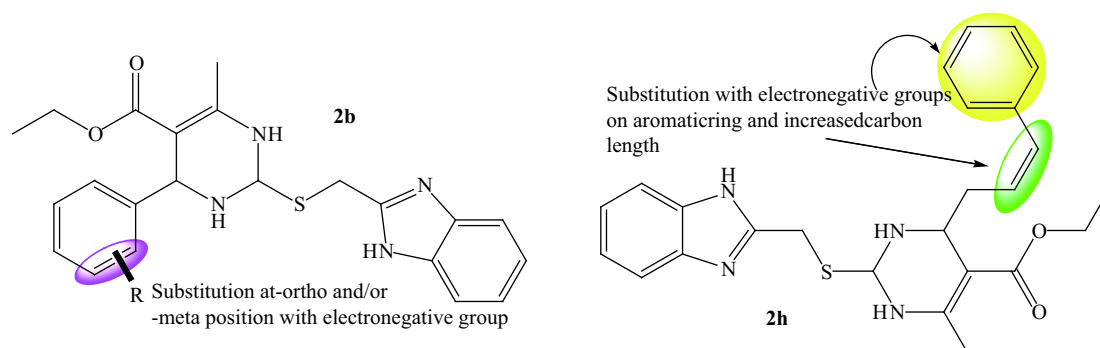
potency. We speculated that substitution with cinnamaldehyde will increase binding affinity as well as the number of hydrogen bonds. The information rendered by molecular docking study improved understanding of the structural requirements for developing more novel blockers of SARS-CoV-2 main protease and inhibitors of the RBD of spike glycoprotein. Figure 5 shows the predicted pharmacophore features of each compound.

Figure 5 Predicted pharmacophore features of novel derivatives for further optimization

5 Conclusion

We could not assess the ability of our derivatives to inhibit SARS-CoV-2 *in vitro* due to safety reasons. However, we investigated their antimicrobial and antifungal properties as preliminary biological evidence. We found that pyrimidine-linked benzimidazole derivatives at specific concentrations were more effective than the standard ampicillin against gram-positive and gram-negative bacteria. Some derivatives were more active at higher concentrations than standard drugs. Gram-negative abcteria *E. coli* and *P. aeruginosa* were more sensitive to the novel derivatives than gram-positive bacteria *S. aureus* and *S. pyogenes*. *C. albicans* was sensitive to the derivatives at a MFC of 250 µg/mL.

The molecular docking method was used to examine whether any possible ligands had potential interactions with the main protease and RBD of spike glycoprotein. Despite certain disadvantages, such as the use of *in vitro* conditions rather than *in vivo* conditions, molecular docking enables researchers to make more accurate decisions in a smaller duration. We developed eight of derivatives that had binding affinity and potential anti SARS-CoV-2 activities that exceeded those of currently approved drugs for treating COVID-19 infection. However, understanding the pharmacophore features of the SARS-CoV-2 main protease and the RBD of spike glycoprotein provides much scope to generate more potent derivatives. Optimizing the properties of these derivatives in models

in vivo and *in vitro*, will lead to more effective options to fight SARS-CoV-2 infection. Because of the critical global COVID-19 situation, we believe that extensive investigation is imperative to acquire a deeper understanding of SARS-CoV-2 and generate effective agents to treat and prevent infection worldwide. At present, a single lead could be a game changer.

Competing interests

The authors declare no conflict of interest.

References

[1] LIU C, ZHOU Q, LI Y, et al. Research and development on therapeutic agents and vaccines for COVID-19 and related human coronavirus diseases. ACS Central Science, 2020, 6(3): 315–331.

[2] SINGH AK, SINGH A, SHAIKH A, et al. Chloroquine and hydroxychloroquine in the treatment of COVID-19 with or without diabetes: a systematic search and a narrative review with a special reference to India and other developing countries. Diabetes and Metabolic Syndrome: Clinical Research and Reviews, 2020, 14(3): 241–246.

[3] ELFIKY AA. Ribavirin, remdesivir, sofosbuvir, galidesivir, and tenofovir against SARS-CoV-2 RNA dependent RNA polymerase (RdRp): a molecular docking study. Life Science, 2020, 117592.

[4] WU D, WU T, LIU Q, YANG Z. The SARS-CoV-2 outbreak: what we know. International Journal of Infectious Diseases, 2020, 94: 44–48.

[5]   NG OW, TAN YJ. Understanding bat SARS-like coronaviruses for the preparation of future coronavirus outbreaks - implications for coronavirus vaccine development. Human Vaccines & Immunotherapeutics, 2017, 13(1): 186–189.

[6]   IBRAHIM IM, ABDELMALEK DH, ELSHAHAT ME, et al. COVID-19 spike-host cell receptor GRP78 binding site prediction. Journal of Infection, 2020, 80(2): 554–562.

[7]   UL QAMAR MT, ALQAHTANI SM, ALAMRI MA, et al. Structural basis of SARS-CoV-2 3CLpro and anti-COVID-19 drug discovery from medicinal plants. Journal of Pharmaceutical Analysis, 2020, 10(4): 313–319.

[8]   WANG W, XU Y, GAO R, et al. Detection of SARS-CoV-2 in different types of clinical specimens. Journal of the American Medical Association, 2020, 323(18): 1843–1844.

[9]   WANG L, WANG Y, YE D, et al. Review of the 2019 novel coronavirus (SARS-CoV-2) based on current evidence. International Journal of Antimicrobial Agents, 2020, 55(6): 105948.

[10] SHEN C, YU N, CAI S, et al. Quantitative computed tomography analysis for stratifying the severity of coronavirus disease 2019. Journal of Pharmaceutical Analysis, 2020, 10(2): 123–129.

[11] LI X, GENG M, PENG Y, et al. Molecular immune pathogenesis and diagnosis of COVID-19. Journal of Pharmaceutical Analysis, 2020, 10(2): 102–108.

[12] CORTEGIANI A, INGOGLIA G, IPPOLITO M, et al. A systematic review on the efficacy and safety of chloroquine for the treatment of COVID-19. Journal of Critical Care, 2020, 57: 279–283.

[13] MAGINNIS MS. Virus-receptor interactions: the key to cellular invasion. Journal of Molecular Biology, 2018, 430(17): 2590–2611.

[14] BOURGONJE AR, ABDULLE AE, TIMENS W, et al. Angiotensin-converting enzyme 2 (ACE2), SARS-CoV-2 and the pathophysiology of coronavirus disease 2019 (COVID-19). Journal of Pathology, 2020, 251(3): 228–248.

[15] ROTHAN HA, BYRAREDDY SN. The epidemiology and pathogenesis of coronavirus disease (COVID-19) outbreak. Journal of Autoimmunity, 2020, 109: 102433.

[16] GUO YR, CAO QD, HONG ZS, et al. The origin, transmission and clinical therapies on coronavirus disease 2019 (COVID-19) outbreak - an update on the status. Military Medical Research, 2020, 7(1): 11.

[17] MUSARRAT F, CHOULJENKO V, DAHAL A, et al. The anti-HIV drug nelfinavir mesylate (viracept) is a potent inhibitor of cell fusion caused by the SARSCoV-2 spike (S) glycoprotein warranting further evaluation as an antiviral against COVID-19 infections. Journal of Medical Virology, 2020, 92(10): 2087–2095.

[18] WEICHUNG J. SHIH, CHEN YAO TX. Data Monitoring for the Chinese clinical trials of remdesivir in treating patients with COVID-19 during the pandemic crisis. Therapeutic Innovation & Regulatory Science, 2020, 54(5): 1–20.

[19] CALY L, DRUCE JD, CATTON MG, et al. The FDA-approved drug ivermectin inhibits the replication of SARS-CoV-2 in vitro. Antiviral Research, 2020, 178: 104787.

[20] JIN Z, DU X, XU Y, et al. Structure of M^{pro} from SARS-CoV-2 and discovery of its inhibitors. Nature, 2020, 582: 289–293.

[21] CRAGG GM, NEWMAN DJ. Natural products: a continuing source of novel drug leads. Biochimica et Biophysica Acta, 2013, 1830(6): 3670–3695.

[22] ALAQEEL SI. Synthetic approaches to benzimidazoles from o-phenylenediamine: a literature review. Journal of Saudi Chemical Society, 2017, 21(2): 229–237.

[23] SHAHARE MB, KADAM VJ, JAGDALE DM, et al. Synthesis and evaluation of novel anthelmentic benzimidazole derivatives. International Journal of Research in Pharmacy and Chemistry, 2012, 2(1): 132–136.

[24] PATIL A, GANGULY S, SURANA S. A systematic review of benzimidazole derivatives as an antiulcer agent. Rasayan Journal of Chemistry, 2008, 1(3): 447–460.

[25] SOLARO RJ, RUEGG JC. Stimulation of Ca++ binding and ATPase activity of dog cardiac myofibrils by AR-L 115BS, a novel cardiotonic agent. Circulation Research, 1982, 51(3): 290–294.

[26] BANSAL Y, SILAKARI O. The therapeutic journey of benzimidazoles: a review. Bioorganic & Medicinal Chemistry, 2012, 20(21): 6208–6236.

[27] FARUK A, DEY BK, CHAKRABORTY A. Synthesis, characterization and pharmacological screening of some novel benzimidazole derivatives. International Research Journal of Pharmacy, 2014, 5(4): 325–331.

[28] CHIMIRRI A, DE SARRO A, DE SARRO G, et al. Synthesis and anticonvulsant properties of 2, 3, 3a, 4-tetrahydro-1H-pyrrolo[1, 2-a]benzimidazol-1-one derivatives. Il Farmaco, 2001, 56(11): 821–826.

[29] AKHTAR W, KHAN MF, VERMA G, SHAQUIQUZZAMAN M, RIZVI MA, MEHDI SH, et al. Therapeutic evolution of benzimidazole derivatives in the last quinquennial period. European Journal of Medicinal Chemistry, 2017, 126: 705–753.

[30] KATRITZKY A, RAMSDEN C, JOULE J, et al. Handbook of Heterocyclic Chemistry. 3rd edition. Elsevier, 2010: 1010.

[31] MAYURA K, CHARAN S. Benzimidazole: an important biological heterocyclic scaffold. Journal of Current Pharma Research, 2014, 4(2): 1159–1167.

[32] AZIZ MA, SERYA RAT, LASHEEN DS, et al. Furo[2, 3-d]pyrimidine based derivatives as kinase inhibitors and anticancer agents. Future Journal of Pharmaceutical Sciences, 2016, 2(1): 1–8.

[33] GOODACRE SC, STREET LJ, HALLETT DJ, et al. Imidazo[1, 2-a]pyrimidines as functionally selective and orally bioavailable GABAAα2/α3 binding site agonists for the treatment of anxiety disorders. Journal of Medicinal Chemistry, 2006, 49(1): 35–38.

[34] PADMAJA A, PAYANI T, REDDY GD, et al. Synthesis, antimicrobial and antioxidant activities of substituted pyrazoles, isoxazoles, pyrimidine and thioxopyrimidine derivatives. European Journal of Medicinal Chemistry, 2009, 44(11): 4557–4566.

[35] UNDHEIM K, BENNECHE T. Pyrimidines and their benzo derivatives. Comprehensive Heterocyclic Chemistry II, 1996, 6: 93–231.

[36] DANSENA H, HJ D, CHANDRAKAR K. Pharmacological potentials of pyrimidine derivative: a review. Asian Journal of Pharmaceutical and Clinical Research, 2015,

8(4): 171–177.

[37] MOHANA ROOPAN S, SOMPALLE R. Synthetic chemistry of pyrimidines and fused pyrimidines: a review. Synthetic Communication, 2016, 46(8): 645–672.

[38] GORDON WG, JOHN AJ. A critical review of the 2005 literature preceded by two chapters on current heterocyclic topics. Progress in Heterocyclic Chemistry, 2007, 18: 126–149.

[39] WANG S, YUAN XH, WANG SQ, et al. FDA-approved pyrimidine-fused bicyclic heterocycles for cancer therapy: synthesis and clinical application. European Journal of Medicinal Chemistry, 2021, 214: 113218.

[40] LAGOJA IM. Pyrimidine as constituent of natural biologically active compounds. Chemistry & Biodiversity, 2005, 2(1): 1–50.

[41] DALLAKYAN S, OLSON AJ. Small-molecule library screening by docking with PyRx. Methods in Molecular Biology, 2015, 1263(1263): 243–250.

[42] RAPPÉ AK, CASEWIT CJ, COLWELL KS, et al. UFF, a full periodic table force field for molecular mechanics and molecular dynamics simulations. Journal of the American Chemical Society, 1992, 114(25): 10024–10035.

[43] CHAUDHARI RN, KHAN SL, CHAUDHARY RS, et al. B-Sitosterol: isolation from muntingia calabura linn bark extract, structural elucidation and molecular docking studies as potential inhibitor of SARS-CoV-2 Mpro (COVID-19). Asian Journal Pharmaceutical and Clinical Research, 2020, 13(5): 204–209.

[44] KHAN SL, SIDDIUI FA. Beta-Sitosterol: as immunostimulant, antioxidant and inhibitor of SARS-CoV-2 spike glycoprotein. Archives of Pharmacology and Therapeutics, 2020, 2(1): 12–16.

[45] KHAN SL, SIDDIQUI FA, JAIN SP, et al. Discovery of potential inhibitors of SARS-CoV-2 (COVID-19) main protease (Mpro) from Nigella Sativa (Black Seed) by molecular docking study. Coronaviruses, 2021, 2(3): 384–402.

[46] DASSAULT SYSTÈMES. Dassault Systèmes BIOVIA, Discovery Studio Modeling Environment. 2017. https://www.3dsbiovia.com/about/citations-references/

[47] GUTIERRÉZ-HERNÁNDEZ A, GALVÁN-CIPRÉS Y, DOMÍNGUEZ-MENDOZA EA, et al. Design, synthesis, antihyperglycemic studies, and docking simulations of benzimidazole-thiazolidinedione hybrids. Journal of Chemistry, 2019, 2019: 1–8.

[48] ALBERT B, ALLAN RD. The preparation of 2-alkylaminobenzimidazoles. The Journal of Organic Chemistry, 1939, 14(17):14-19.

[49] SHEN ZL, XU XP, JI SJ. Brønsted base-catalyzed one-pot three-component Biginelli-type reaction: an efficient synthesis of 4,5,6-triaryl-3,4-dihydropyrimidin-2(1H)-one and mechanistic study. Journal of Organic Chemistry, 2010, 75(4): 1162–1167.

[50] DURGA DEVI D, MANIVARMAN S, SUBASHCHANDRABOSE S. Synthesis, molecular characterization of pyrimidine derivative: a combined experimental and theoretical investigation. Karbala International Journal of Modern Science, 2017, 3(1): 18–28.

[51] BAELL J, CONGREVE M, LEESON P, et al. Ask the experts: past, present and future of the rule of five. Future Medicinal Chemistry, 2013, 5(7): 745–752.

[52] GIMÉNEZ BG, SANTOS MS, FERRARINI M, et al. Evaluation of blockbuster drugs under the rule-of-five. Archiv der Pharmazie, 2010, 65(2): 148–152.

[53] WALTERS WP. Going further than Lipinski's rule in drug design. Expert Opinion on Drug Discovery, 2012, 7(2): 99–107.

[54] NENDZA M, MÜLLER M. Screening for low aquatic bioaccumulation (1): Lipinski's "rule of 5" and molecular size. SAR and QSAR in Environmental Research, 2010, 21(5-6): 495–512.

[55] BALOUIRI M, SADIKI M, IBNSOUDA SK. Methods for in vitro evaluating antimicrobial activity: a review. Journal of Pharmaceutical Analysis, 2016, 6(2): 71–79.

[56] RAHMAN M, HASAN MF, DAS R, et al. The determination of antibacterial and antifungal activities of Polygonum hydropiper (L.) root extract. Advances in Biological Research, 2009, 3(2): 53–56.

[57] BHALODIA NR, NARIYA PB, SHUKLA VJ. Antibacterial and antifungal activity from flower extracts of Cassia fistula L.: an ethnomedicinal plant. International Journal of PharmTech Research, 2011, 3(1): 160–168.

新型嘧啶-苯并咪唑杂合物的抗细菌和抗真菌特性及其对新冠病毒主要蛋白酶和刺突糖蛋白的潜在抑制作用

Sharuk Khan[a*], Mayura Kale[b], Falak Siddiqui[a], Nitin Nema[c]

a. Department of Pharmaceutical Chemistry, MUP's College of Pharmacy (B Pharm), Washim, Maharashtra 444504, India

b. Department of Pharmaceutical Chemistry, Government College of Pharmacy, Aurangabad, Maharashtra 431003, India

c. Department of Pharmacology, Shri Vile Parle Kelavani Mandal's (SVKM's) Institute of Pharmacy, Dhule, Maharashtra 424001, India

【摘要】目的 本研究旨在合成和表征嘧啶连接的苯并咪唑杂环化合物,确定其体外抗微生物和抗真菌活性,并测定其抑制新冠病毒主要蛋白酶和刺突糖蛋白的能力。方法 利用分子对接技术,通过评估苯并咪唑杂环合成化合物与酶的变构位点的结合方式,研究其抑制新冠病毒主要蛋白酶和刺突糖蛋白的能力。通过光谱分析验证了微波辅助合成的嘧啶连接苯并咪唑衍生物的结构。通过肉汤稀释法测定其抗细菌和抗真菌活性。结果 革兰氏阴性大肠杆菌和铜绿假单胞菌对这些衍生物的敏感性高于革兰氏阳性金黄色葡萄球菌和化脓性链球菌。白色念珠菌在最低抑菌浓度 250 μg/mL 下对这些衍生物敏感。相比目前作为新冠病毒感染疗法进行研究的奈非那韦、洛匹那韦、伊维菌素、瑞德西韦和法匹拉韦,这些新型衍生物具有更好的结合亲和力 (kcal/mol),目前正在研究这些药物治疗新冠病毒感染。化合物 2c、2e 和 2g 与主蛋白酶的活性空腔形成四个氢键。许多衍生物对新冠病毒刺突糖蛋白的受体结合域 (RBD) 具有良好的结合亲和力,最多可形成四个氢键。结论 我们合成了一些新型的嘧啶连接苯并咪唑衍生物,它们是强效的抗微生物制剂,具有抑制新冠病毒刺突糖蛋白的能力。了解主要蛋白酶和刺突糖蛋白的药效团特征为开发更强效的药物提供了广阔空间。我们计划使用体内和体外模型优化这些衍生物的性质,使它们成为更有效的抗细菌和新冠病毒感染的治疗选择。

【关键词】新型冠状病毒抑制剂;新型冠状病毒肺炎;分子对接;嘧啶-苯并咪唑;细菌;抗真菌